

pubs.acs.org/Biomac Article

# Controlled Dissociation of Polymeric Micelles in Response to Oxidative Stress

Roujia Chang, Binru Han, Amira Ben Mabrouk, and Urara Hasegawa\*



Cite This: https://doi.org/10.1021/acs.biomac.3c01156



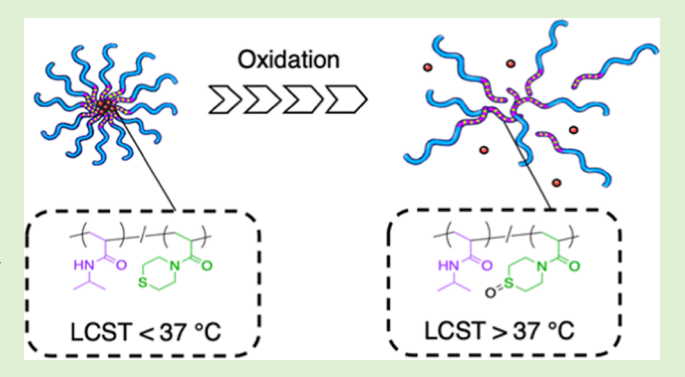
**ACCESS** 

III Metrics & More

Article Recommendations

s Supporting Information

ABSTRACT: Nanoparticle-based drug carriers that can respond to oxidative stress in tumor tissue have attracted attention for site-specific drug release. Taking advantage of the characteristic microenvironment in tumors, one of the attractive directions in drug delivery research is to design drug carriers that release drugs upon oxidation. A strategy to incorporate oxidation-sensitive thioether motifs such as thiomorpholine acrylamide (TMAM) to drug carriers has been often used to achieve oxidation-induced dissociation, thereby targeted drug release. However, those delivery systems often suffer from a slow dissociation rate due to the intrinsic hydrophobicity of the thioether structures. In this study, we aimed to enhance the dissociation rate of TMAM-based micelles upon oxidation. The random copolymers of N-



isopropylacrylamide and TMAM (P(NIPAM/TMAM)) were designed as an oxidation-sensitive segment that showed a fast response to oxidative stress. We first synthesized P(NIPAM/TMAM) copolymers with different NIPAM:TMAM molar ratios. Those copolymers exhibited low critical solution temperatures (LCSTs) below 32 °C, which shifted to higher temperatures after oxidation. The changes in LCSTs depend on the NIPAM:TMAM molar ratios. At the NIPAM:TMAM molar ratio of 82:18, the LCSTs before and after oxidation were 17 and 54 °C, respectively. We then prepared micelles from the diblock copolymers of poly(N-acryloyl morpholine) (PAM) and P(NIPAM/TMAM). The micelles showed an accelerated dissociation rate upon oxidation compared to the micelles without NIPAM units. Furthermore, the doxorubicin (Dox)-loaded micelles showed enhanced relative toxicity in human colorectal cancer (HT29) cells over human umbilical vein endothelial cells (HUVECs). Our novel strategy to design an oxidation-sensitive micellar core comprising a P(NIPAM/TMAM) segment can be used as a chemotherapeutic delivery system that responds to an oxidative tumor microenvironment in an appropriate time scale.

#### 1. INTRODUCTION

Tumors are known to have an oxidative microenvironment due to an elevated concentration of reactive oxygen species (ROS) such as hydroxyl radicals (\*OH), superoxide (O2\*-), peroxyl radicals (ROO\*), hydrogen peroxide (H2O2), and singlet oxygen (1O2). 1,2 Upregulated ROS production in cancer cells is due to an increase in metabolic activity, oncogenic stimulation, mitochondrial malfunction, increased activity of oxidases, and other deregulation of antioxidant systems. ROS is mainly produced in mitochondria through electron transport to oxygen molecules by the actions of a series of enzymes. ROS plays a key role as a signaling molecule regulating the activities of proteins such as transcription factors, protein tyrosine phosphatases, and receptor and nonreceptor protein tyrosine kinases through reversible oxidation.

In the field of drug delivery research, the overproduction of ROS in the tumor microenvironment has been exploited as a "biomarker" for targeting tumor tissue. Thus far, significant efforts have been made to develop drug carriers containing an oxidation-sensitive motif, which alters its water solubility or degrades upon oxidation. Thioether-containing polymers are

one of the widely used oxidation-sensitive building blocks that can be oxidized to more polar sulfoxides, thereby undergoing a hydrophobic-to-hydrophilic phase transition upon oxidation. It has been demonstrated that polymeric micelles and vesicles with a core bearing thioether groups  $^{11,12}$  and other oxidation-sensitive motifs  $^{13-21}$  were destabilized in the presence of hydrogen peroxide (H<sub>2</sub>O<sub>2</sub>), one of the most dominant ROS in the body.  $^{7,22-24}$  To further explore the potential of the oxidation-sensitive drug carriers, our group investigated the influence of the chemical structure of thioethers on the oxidation sensitivity of micelles. We prepared polymeric micelles with a core containing different thioether groups, such as 3-methylthiopropylacrylamide, thiomorpholine acryl-

Received: October 24, 2023 Revised: January 8, 2024 Accepted: January 8, 2024



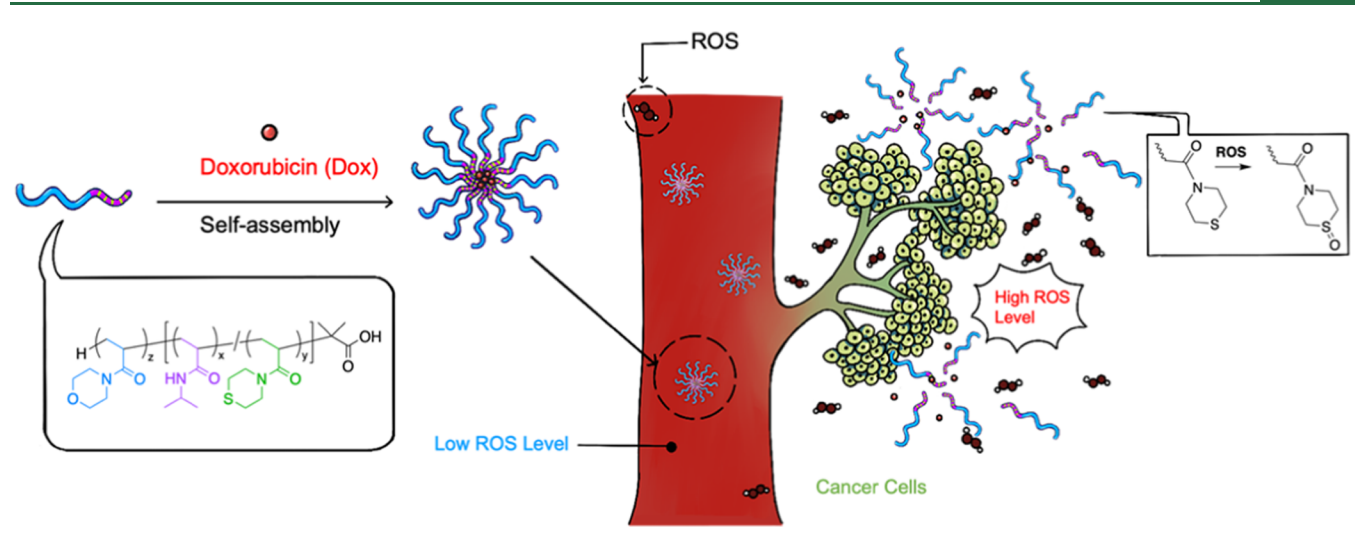


Figure 1. Oxidation-sensitive polymeric micelles with a controlled dissociation rate. The micelles prepared from PAM-(PNIPAM/TMAM) amphiphilic block copolymers show a rapid response to the elevated ROS levels, resulting in micelle dissociation and drug release.

amide (TMAM), and 4-(methylthio)benzyl acrylamide, <sup>25</sup> and found that the micelles containing TMAM showed highest selectivity toward human liver cancer HepG2 cells over human umbilical vein endothelial cells (HUVECs). The results clearly show the importance of fine-tuning the oxidation sensitivity of thioether structures in order to achieve cancer-selective targeted drug delivery. However, those micelles showed a relatively slow dissociation rate within cells (more than 2 days in HepG2 cells), which poses a concern since the slow drug release can result in the development of drug resistance in cancer. Although the oxidation of thioether groups increases their polarity, this may not be enough for the polymers to be hydrated completely. Therefore, the micelle's slow response to ROS seems to be due to the intrinsic hydrophobicity of thioether structures.

In this paper, we present a novel design to improve the dissociation rate of TMAM-based polymeric micelles. To facilitate micelle dissociation, we focused on poly(Nacrylamide) (PNIPAM), which is a thermosensitive polymer that exhibits a rapid coil-to-globule transition in water above its low critical solution temperature (LCST) of 32 °C. PNIPAM is a thermosensitive polymer that is soluble in water (coil) below 32 °C but becomes insoluble (globule) above this temperature. It is known that the LCST of PNIPAM can be controlled by copolymerizing NIPAM with other comonomers.<sup>26–31</sup> When the comonomer is hydrophobic, the LCST of the PNIPAM copolymer decreases below 32 °C. In the case of hydrophilic comonomers, the LCST of the copolymer becomes higher than 32 °C. Recently, Valencia and coworkers reported random copolymers of NIPAM and thioether-containing monomers, 6-(methylthio)hexyl acrylate or 2-(methylthio)ethyl acrylate, and showed that the LCSTs of these copolymers increased upon oxidation of thioethers to sulfoxides.<sup>32</sup> However, the LCST values for the polymers after oxidation were below 30 °C, which is much lower than body temperature. Therefore, careful selection of thioether groups as well as copolymer compositions is needed to optimize the compounds for biomedical applications. Here, we developed a new oxidation-sensitive polymer by copolymerizing Nisopropylacrylamide (NIPAM) and TMAM at different NIPAM:TMAM ratios. We hypothesized that the LCST of P(NIPAM/TMAM) copolymers can be optimized by screen-

ing the different NIPAM:TMAM ratios. The LCST of the P(NIPAM/TMAM) copolymer is expected to be lower than that of the PNIPAM homopolymer (32 °C) due to the nonpolar nature of TMAM groups, and therefore, the copolymers will be insoluble in water at body temperature (37 °C). Upon oxidation, nonpolar TMAM will be converted to the corresponding sulfoxide, which is more polar than thioether (Figure 1), resulting in an increase in the LCST, thereby causing polymer dissolution in water. The P(NIPAM/ TMAM) random copolymers with different compositions of NIPAM and TMAM were synthesized by reversible additionfragmentation chain-transfer (RAFT) polymerization, and their LCSTs before and after oxidation were determined by turbidity measurement. Then, the poly(N-acryloyl morpholine)-P(NIPAM/TMAM) amphiphilic diblock copolymers (PAM-P(NIPAM/TMAM)) were synthesized and used to prepare the micelles by self-assembly in water at 37 °C. The dissociation rate of the PAM-P(NIPAM/TMAM) micelles was compared with the micelles without NIPAM units (PAM-PTMAM) after incubation with  $H_2O_2$ . Furthermore, micelles loaded with doxorubicin (Dox) were used to evaluate their cytotoxicity in human colorectal cancer (HT29) cells as well as in HUVECs.

#### 2. EXPERIMENTAL SECTION

2.1. Synthesis of Poly(N-isopropylacrylamide/N-acryloyl thiomorpholine) Random Copolymers (P(NIPAM/TMAM)) (1a-d). NIPAM was copolymerized with TMAM by RAFT polymerization using azobis(isobutyronitrile) (AIBN) as the initiator and 2-(dodecylthiocarbonothioylthio)-2-methylpropionic acid as the chain-transfer agent (CTA) (Table S1). A typical procedure to synthesize 1d: NIPAM (362.1 mg, 3.20 mmol), TMAM (127.4 mg, 0.80 mmol), AIBN (0.657 mg, 0.004 mmol), and CTA (14.6 mg, 0.040 mmol) were dissolved in distilled 1,4-dioxane (total volume: 2 mL) in a Schlenk tube. Five freeze-pump-thaw cycles under argon were performed to remove oxygen. The reaction mixture was placed in an oil bath at 60 °C and stirred for 24 h. The polymerization reaction was terminated by placing the Schlenk tube in liquid nitrogen and exposing the reaction mixture to air. The solution was added dropwise to 40 mL of hexane. The polymers were collected by filtration, washed with hexane (3 × 15 mL), and dried under reduced pressure at 40 °C to yield a yellow solid (418.7 mg, 84.6% for 1d). The polymers were characterized by proton nuclear magnetic resonance (<sup>1</sup>H NMR) and gel permeation chromatography (GPC).

Scheme 1. Synthesis Scheme of Thioether-Conjugated P(NIPAM/TMAM) Random Copolymer; AIBN, 1,4-Dioxane, 60 °C, 24 ha

<sup>a</sup>x: degree of polymerization of NIPAM, y: degree of polymerization of TMAM.

2.2. Synthesis of Poly(N-acryloyl morpholine)-P(NIPAM/TMAM) Diblock Copolymers (PAM-P(NIPAM/TMAM)) (2). PAM-P(NIPAM/TMAM) was synthesized by RAFT polymerization with AIBN as the initiator and P(NIPAM/TMAM) as the macro CTA (Table S2). For 2d, AM (141.2 mg, 1.0 mmol), P(NIPAM/TMAM) (63.0 mg, 0.005 mmol), and AIBN (0.082 mg, 0.0005 mmol) were dissolved in 1,4-dioxane (total volume: 2.5 mL). Five freeze-pump-thaw cycles under argon were performed to remove oxygen. The reaction mixture was placed in an oil bath at 60 °C. After 24 h of reaction, the solution was added dropwise to 50 mL of diethyl ether (Et<sub>2</sub>O). The polymers were collected by filtration, washed with Et<sub>2</sub>O (3 × 17 mL), and dried under vacuum to yield the lightyellowish solid (176.1 mg, 86.3%). The polymers were characterized by  $^1$ H NMR and GPC.

2.3. CTA End Group Removal of PAM-P(NIPAM/TMAM) Diblock Copolymers (3b–e). The CTA end group was removed by radical-induced reduction with AIBN as the initiator (Table S3). For 3d, polymer 2d (115 mg, 0.0028 mmol), AIBN (0.9 mg, 0.0056 mmol), and tris(trimethylsilyl)silane (3.5 mg, 4.32  $\mu$ L, 0.0141 mmol) were dissolved in 1,4-dioxane (total volume: 2 mL). The light-yellow solution was deoxygenated by five freeze–pump—thaw cycles under argon and placed in an oil bath at 70 °C. After 24 h of reaction, the solution became colorless and was added dropwise to 40 mL of diethyl ether (Et<sub>2</sub>O). The polymers were collected by filtration, washed with Et<sub>2</sub>O (3 × 15 mL), and dried under vacuum to yield the white solid (97.5 mg, 84.8%). The polymers were characterized by  $^1$ H NMR and GPC.

**2.4. LCST Determination by Turbidity Measurement.** Random copolymers **1b**, **1c**, and **1d** were dissolved in phosphate-buffered saline (PBS) (100 mM, pH 7.4) at 4 mg/mL. For  $\rm H_2O_2$ -treated samples, the polymer solutions were incubated with 0.3 wt %  $\rm H_2O_2$  at room temperature for 24 h. The transmittance at 500 nm was measured at different temperatures (5–56 °C) using a UV–vis spectrometer. The sample temperature was increased stepwise. The LCST was determined by calculating the temperature for 50% transmittance by linear interpolation.

**2.5. Micelle Preparation.** Diblock copolymers 3b-d were dissolved in PBS (100 mM, pH 7.4), and micelle formation induced by the temperature gradient was characterized. The size distribution of micelles was measured at 25 and 37 °C by dynamic light scattering (DLS) at a concentration of 1 mg/mL. For measurements at 37 °C, the polymer solutions were incubated at 37 °C for 5 min. In the case of 3e, the polymer was dissolved in *N*-methyl pyrrolidone (NMP) at 50 mg/mL and added dropwise to distilled water under stirring (volume fraction (v/v) of NMP = 10%; final concentration of the polymer: 5 mg/mL). After stirring for 1 day at room temperature, the solution was dialyzed (dialysis membrane tubing, MWCO 3.5 kDa) against 1 L of distilled water for 4 days. The dialysis water was replaced regularly.

**2.6.** Micelle Dissociation upon H<sub>2</sub>O<sub>2</sub> Treatment at 37 °C. Diblock copolymers 3b—e at a concentration of 1 mg/mL in PBS (pH 7.4, 100 mM) were treated with H<sub>2</sub>O<sub>2</sub> at different concentrations (0, 0.003, 0.03, and 0.1 wt %). The size distribution of micelles was measured by DLS at 37 °C. Before measurements at 37 °C, the micelles were incubated at 37 °C for 5 min. Furthermore, the micelle dissociation of 3d was observed by transmission electron microscopy (TEM). The 3d solution in PBS at 1 mg/mL was incubated at 37 °C

for 1d and thereafter incubated with 0.03 and 0.1 wt %  $H_2O_2$  for 1d before preparing grids for TEM.

**2.7. Cell Culture.** The human colorectal adenocarcinoma HT29 cell was cultured in McCoy's 5A medium supplemented with 10% fetal bovine serum and penicillin–streptomycin (P/S, 100 U/mL to 100  $\mu$ g/mL) in a 5% CO<sub>2</sub> incubator at 37 °C. The human umbilical vein endothelial cell line HUVEC was cultured in human large vessel endothelial cell basal medium supplemented with LSGS and P/S (10 U/mL to 10  $\mu$ g/mL) in a 5% CO<sub>2</sub> incubator at 37 °C.

**2.8.** Dox Encapsulation in the Micelles. Lyophilized 3d was dissolved in distilled water at a concentration of 6 mg/mL. Dox·HCl was dissolved in dimethyl sulfoxide (DMSO) at 10 mM, and 0.7  $\mu$ L of triethylamine (TEA) was added to 500  $\mu$ L of the Dox·HCl solution to deprotonate Dox. The 3d polymer solution (6 mg/mL) was mixed with the deprotonated Dox solution to prepare Dox/3d solutions at Dox concentrations of 1, 0.7, 0.5, 0.3, and 0.2 mM. The Dox/3d solutions were incubated at 37 °C for 10 min and filtered through a 0.22  $\mu$ M syringe filter. The filtered solution was further incubated at 37 °C overnight. The size distribution of Dox-loaded micelles was measured by DLS at 37 °C.

**2.9.** Preparation of Dox-Loaded Micelles for Cytotoxicity Assay. The lyophilized 3d polymer was dissolved in cell culture grade water at a concentration of 6 mg/mL. 18.66  $\mu$ L portion of the deprotonated Dox solution (10 mM) was added dropwise to 1 mL of the 3d polymer solution and stirred for 30 min at room temperature, with subsequent incubation at 37 °C for 30 min. The Dox/3d solution was stored at -20 °C.

**2.10. Determination of the Dox Concentration.** A serial dilution was performed to prepare a standard curve of deprotonated Dox in a DMSO/water mixture (90% DMSO, 10% water). The absorbance of solutions at 500 nm was measured by UV—vis spectroscopy. The Dox-loaded micelle solution was mixed with DMSO at a volume ratio of 1:9, and the concentration was determined using the standard curve.

**2.11.** Intracellular Dox Release. HT29 cells were seeded at 5  $\times$  10<sup>3</sup> cells/well in a 4-well glass bottom dish and cultured for 2 days. The medium was replaced with 200  $\mu$ L/well of a fresh medium containing Hoechst 33342 dye (8  $\mu$ M). After 15 min of incubation, the medium was replaced with 200  $\mu$ L/well of a fresh medium containing Dox or Dox-loaded micelles (Dox concentration: 10  $\mu$ M). After 1.5 or 3 h of incubation in a CO<sub>2</sub> incubator, the medium was replaced with 200  $\mu$ L/well of a fresh medium. Cells were observed by confocal laser scanning fluorescence microscopy (CLSFM).

**2.12. Cytotoxicity of Dox-Loaded Micelles.** HT29 cells and HUVECs were seeded in a 96-well plate (HT29:  $5.0 \times 10^3$  cells/well, HUVEC:  $2.0 \times 10^3$  cells/well) and cultured for 1 day. The cell culture medium was mixed with Dox/3d solution at different concentrations at the volume ratio of 9:1 and incubated at 37 °C for 20 min before adding to cells. A medium containing free Dox was also prepared by mixing the medium with Dox-HCl/DMSO solution at different concentrations (final DMSO concentration: 1%). After the medium was replaced with 50  $\mu$ L/well of a fresh medium containing Dox/3d or Dox-HCl, the cells were cultured for 3 days in a CO<sub>2</sub> incubator. The medium was replaced with 100  $\mu$ L of 0.5 mg/mL 3-(4,5-dimethylthiazol-2-yl)-2,5-diphenyltetrazolium bromide (MTT) in the medium. The cells were cultured for 5 h, and the formazan crystals

were dissolved in 100  $\mu$ L/well of a 100 mg/mL sodium dodecyl sulfate solution in 0.01 M HCl (aq). The absorbance at 570 nm was measured by using a microplate reader. Metabolic activity was expressed as % of the absorbance of the nontreated samples. The IC  $_{50}$  of HT29 cells and HUVECs was determined using a two-parameter logistic regression model:

% metabolic activity = 
$$\frac{100}{1 + \left(\frac{C}{IC_{50}}\right)^n}$$
 (1)

where C is the Dox concentration and n is the Hill coefficient. The cytotoxicity of Dox/3a in HT29 cells was also evaluated.

# 3. RESULTS AND DISCUSSION

**3.1. Synthesis of P(NIPAM/TMAM) Random Copolymers.** The polymers were synthesized by RAFT polymerization, as shown in Scheme 1. P(NIPAM/TMAM) random copolymers  $1\mathbf{b}-\mathbf{d}$  were synthesized at different NIPAM:T-MAM molar ratios. PNIPAM homopolymer  $1\mathbf{a}$  and PTMAM homopolymer  $1\mathbf{e}$  were prepared as controls. HNMR (Figures S2–S5) was used to determine the NIPAM:TMAM ratios based on the integral values of the peaks at around 4.0 and 3.6 ppm. The NIPAM:TMAM ratio of each copolymer determined by HNMR was nearly equal to the monomer ratio showing successful synthesis of the P(NIPAM/TMAM) copolymers  $1\mathbf{b}-\mathbf{d}$ . As determined by GPC, the synthesized polymers had a dispersity index  $(M_w/M_n)$  of 1.01-1.04 showing narrow size distribution (Table 1 and Figures S6 and S7).

Table 1. Characterization of P(NIPAM/TMAM)

molar ratio, x:y					
entry	theoretical	experimental <sup>a</sup>	$M_{\rm w}^{}$ [g/mol]	$M_{\rm n}^{\ b} \left[ {\rm g/mol} \right]$	$M_{\rm w}/M_{\rm n}^{}$
1a	100:0	100:0	$9.18 \times 10^{3}$	$9.08 \times 10^{3}$	1.01
1b	95:5	97:3	$9.73 \times 10^{3}$	$9.39 \times 10^{3}$	1.04
1c	90:10	90:10	$9.79 \times 10^{3}$	$9.66 \times 10^{3}$	1.01
1d	80:20	82:18	$1.60 \times 10^{4}$	$1.55 \times 10^{4}$	1.04
1e	0:100	0:100	$1.98 \times 10^{4}$	$1.95 \times 10^{4}$	1.02

<sup>a</sup>Determined by <sup>1</sup>H NMR. <sup>b</sup>Determined by GPC-multiangle light scattering (MALS) detection. Eluent: tetrahydrofuran (THF).

3.2. LCST Before and After Oxidation. The random copolymers 1a-d were dissolved in PBS (100 mM) and treated with/without 0.3 wt % H<sub>2</sub>O<sub>2</sub> for 1 day. The transmittance at 510 nm was measured at different temperatures. The LCST was determined by linear interpolation at 50% transmittance (Figures 2, S8, and Table 2). The LCSTs of all copolymers of NIPAM and TMAM were below 32 °C with more TMAM units showing a lower LCST. This is due to the incorporation of the hydrophobic comonomer (TMAM), which is known to decrease the LCST. On the other hand, incubation of those polymers with 0.3 wt % H<sub>2</sub>O<sub>2</sub> significantly increased their LCSTs. Importantly, polymers with higher TMAM contents showed higher LCSTs upon oxidation. The results clearly showed that the increase in polarity of TMAM units after oxidation affected the LCST significantly. For example, 1d, which contains 18 mol % TMAM, showed the lowest LCST (17.3 °C) before oxidation, but the highest LCST (53.7 °C) after oxidation. This means that this polymer is insoluble at body temperature (37 °C) before oxidation but becomes soluble after oxidation. The results supported our hypothesis that the LCST of the P(NIPAM/TMAM)

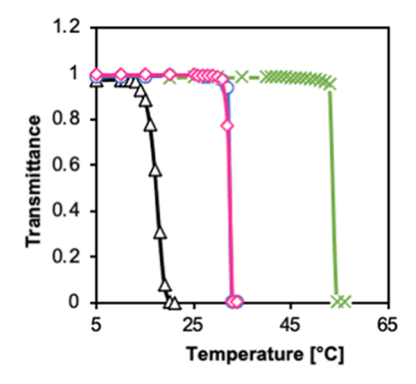


Figure 2. Turbidity measurement of 1d and 1a before and after 0.3 wt %  $H_2O_2$  treatment for 24 h incubation in PBS (pH 7.4, 100 mM). Transmittance at 500 nm was measured. Black  $\triangle$ : 1d,  $H_2O_2$  (-); green  $\times$ : 1d,  $H_2O_2$  (+); blue O: 1a,  $H_2O_2$  (-); and magenta  $\diamondsuit$ : 1a,  $H_2O_2$  (+).

Table 2. LCSTs of P(NIPAM/TMAM) Polymers after 1 Day of Incubation with and without H<sub>2</sub>O<sub>2</sub>

	LCST [°C]		
entry	without H <sub>2</sub> O <sub>2</sub>	0.3 wt % H <sub>2</sub> O <sub>2</sub>	
la	32.4	32.4	
1b	29.4	35.5	
1c	25.4	41.7	
1d	17.3	53.7	

copolymer can be increased by the oxidation of TMAM groups.

To further confirm that the LCST change is due to the oxidation of TMAM groups, the polymers before and after incubation with 0.3 wt %  $\rm H_2O_2$  were characterized by  $^1\rm H$  NMR and Fourier transform infrared spectroscopy (FT-IR). The  $^1\rm H$  NMR spectra showed peaks at 2.8 and 4.5 ppm, indicating sulfoxide formation (Figure S9). It should be noted that 1a (PNIPAM) did not show any change upon  $\rm H_2O_2$  incubation. The stretching vibration at 1005 cm $^{-1}$  for TMAM in the FT-IR spectra further confirmed the formation of the sulfoxide group (S=O) after  $\rm H_2O_2$  incubation for 1b, 1c, and 1d (Figure S10).  $^{25}$ 

3.3. Synthesis of PAM-P(NIPAM/TMAM) Diblock Copolymers. Having prepared the oxidation-sensitive P-(NIPAM/TMAM) polymers, we next prepared block copolymers comprising a hydrophilic poly(N-acryloyl morpholine) (PAM) block and an oxidation-sensitive P(NIPAM/TMAM) block (Scheme 2). N-acryloyl morpholine (AM) was polymerized using copolymers 1b-e as the macro CTA to obtain diblock copolymers **2b−e**. The number of units of PAM relative to P(NIPAM/TMAM) was determined using the integral values of the peaks at 4.00, 3.63, and 3.30 ppm in the <sup>1</sup>H NMR spectra (Figures S11-S20). As shown in Table 3, the z:(x + y) ratios of the polymers 2b-d were similar to the feed ratio (i.e., 200:100), showing that the reaction proceeded quantitatively. In addition, the polymers 2b-d showed a relatively narrow size distribution with the  $M_w/M_n$  values of 1.04-1.08 as determined by GPC (Table 3 and Figures S21-S25). Those results indicate the successful synthesis of PAM-P(NIPAM/TMAM) block copolymers by RAFT polymerization. In the case of PAM-PTMAM 2e, the AM length was shorter, and the resulting polymer showed a broader size distribution, as shown in Figure S25. This indicates that

Scheme 2. Synthesis Scheme of Thioether-Conjugated PAM-P(NIPAM/TMAM) Diblock Copolymers<sup>a</sup>

"(i) AIBN, 1,4-dioxane, 60 °C, 24 h; (ii) tris(trimethylsilyl)silane, AIBN, 1,4-dioxane, 70 °C, 24 h. Subscript z = degree of polymerization of AM; x = degree of polymerization of NIPAM; and y = degree of polymerization of TMAM.

Table 3. Characterization of PAM-P(NIPAM/TMAM) Diblock Copolymers<sup>b</sup>

	molar ratio, $z$ : $(x + y)$				
entry	theoretical	experimental <sup>a</sup>	$M_{ m w} \left[ { m TC6}  ight] \left[ { m g/mol}  ight]$	$M_{\rm n}$ [TC7] [g/mol]	$\frac{M_{\rm w}/M_{\rm n}}{[{ m TC8}]}$
2a	200:100	185:0	$2.83 \times 10^{4}$	$2.75 \times 10^{4}$	1.03
2b	200:100	196:100	$3.25 \times 10^{4}$	$3.02 \times 10^{4}$	1.08
2c	200:100	201:100	$2.83 \times 10^{4}$	$2.73 \times 10^4$	1.04
2d	200:100	191:100	$3.35 \times 10^{4}$	$3.24 \times 10^4$	1.07
2e	200:100	163:100	$6.11 \times 10^4$	$3.82 \times 10^4$	1.60
$^a\mathrm{Determined}$ by $^1\mathrm{H}$ NMR. $^b\mathrm{Determined}$ by GPC-MALS. Eluent				Eluent:	

THF.

termination occurred during polymerization. The CTA end group was then removed by radical-induced reduction to yield copolymers 3b-e. Successful CTA end group removal was confirmed by the absence of the peak in <sup>1</sup>H NMR spectroscopy (0.90 ppm).

3.4. Preparation of the Micelles. The micelles were prepared from the diblock copolymers 3b-e by self-assembly of the core-forming P(NIPAM/TMAM) segment at 37 °C. As discussed above, the P(NIPAM/TMAM) copolymers 1b-d have LCSTs at 17-30 °C. Therefore, the diblock copolymers 3b-e are expected to form micelles at 37 °C since the P(NIPAM/TMAM) block becomes insoluble in water at this temperature (Figure 3). The micelle formation was confirmed



Figure 3. Self-assembly of thermosensitive NIPAM-conjugated amphiphilic polymers 3b-d at temperatures above the LCST.

at 37 °C by DLS (Figure S26). For 3b and 3c polymers, a small peak around 10 nm was also observed at 37 °C, along with the peak due to the micelles. This could be due to the low thermodynamic stability of the 3b and 3c micelles. As shown in Table 4, the average hydrodynamic diameters of micelles 3b−d at 37 °C were 50−60 nm. As shown by negative staining TEM, polymers 3b-d formed spherical micelles (Figure 4). Furthermore, the micelles of polymer 3e were prepared by the nanoprecipitation method as described previously. 25 Negative staining TEM showed that polymer 3e formed rodlike/

Table 4. Size Distribution of the Micelles Prepared from PAM-P(NIPAM/TMAM) Polymers at 37 °C

entry	$D_{\rm h}^{a}$ [nm]	PDI <sup>b</sup>
3b	52.4	0.32
3c	60.6	0.31
3d	50.3	0.08
3e	18.7	0.39

<sup>a</sup>Z-average hydrodynamic diameter as determined from the cumulant fit (DLS). <sup>b</sup>Polydispersity index as determined from the cumulant fit (DLS). The micelles were dispersed in PBS (pH 7.4, 100 mM).

cylindrical micelles (Figure 4d), which seems to be the reason for the high PDI value for the 3e micelles.

3.5. Dissociation of the Micelles upon Oxidation. Dissociation of the micelles in the presence of H<sub>2</sub>O<sub>2</sub> was evaluated. As shown in Figure 5, for 3d micelles, the decrease in the scattered light intensity was observed after 1 h of incubation with 0.03 wt % H<sub>2</sub>O<sub>2</sub>, and the micelle structure disappeared completely after 24 h. In contrast, 3e micelles retained its structure even after 24 h. In addition, the faster dissociation of the micelles was observed at different H<sub>2</sub>O<sub>2</sub> concentrations (0.003 and 0.1 wt %) (Figure S27). A similar trend was also observed for other micelles 3b and 3c (Figure S28). It should be noted that the micelles with the lowest TMAM content (3b, 3%) showed the fastest dissociation, followed by 3c (10%) and 3d (18%). Furthermore, for 3b and 3c (Figure S28), the large structures were observed after incubation at high H<sub>2</sub>O<sub>2</sub> concentration, which seems to be due to aggregated or swollen structures of partially oxidized micelles.

We plotted the decrease in the scattered light intensity as a function of H2O2 concentrations to show the H2O2 concentration-dependent micelle dissociation after 1 h of incubation (Figure S29). The scattered light intensity of the 3b micelles decreased to ~70% (relative to the nontreated micelles) at 0.003 wt % H<sub>2</sub>O<sub>2</sub> and further decreased with the increase of H<sub>2</sub>O<sub>2</sub> concentration. The 3c micelles were less sensitive to oxidation compared to the 3b micelles, but also showed a slight decrease in intensity at 0.003 wt % H<sub>2</sub>O<sub>2</sub>. On the other hand, as for the 3d micelles, we only observed a clear decrease in the scattering intensity at 0.03 wt % H<sub>2</sub>O<sub>2</sub>. Furthermore, we observed the micelle morphology of the 3d micelles after 1 day of incubation in PBS containing 0.03 and 0.1 wt % H<sub>2</sub>O<sub>2</sub> by TEM. As shown in Figure S30, the

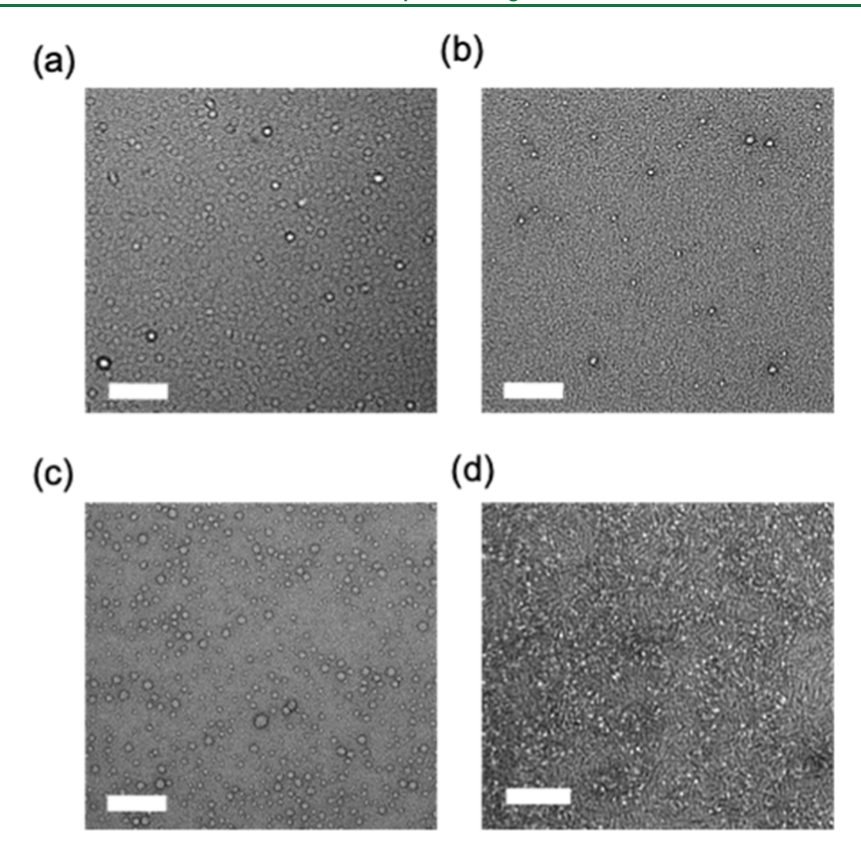
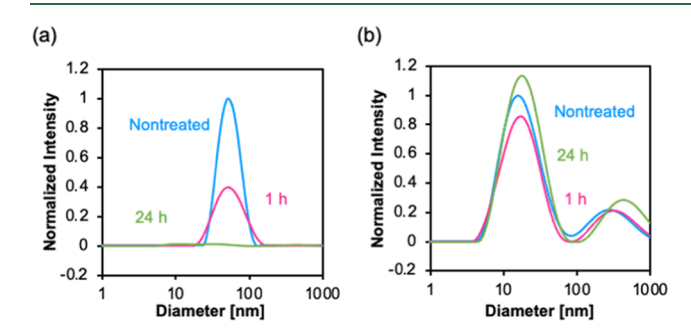


Figure 4. Negative staining TEM images of (a) 3b, (b) 3c, (c) 3d, and (d) 3e. The micelle solutions were incubated for 24 h at 37 °C and placed on TEM grids, followed by negative staining with 2 wt % uranyl acetate. Scale bar: 200 nm.



**Figure 5.** Micelle size distribution of (a) **3d** and (b) **3e** measured by DLS in PBS (pH 7.4, 100 mM) at 37  $^{\circ}$ C after 0.03 wt %  $H_2O_2$  treatment for 1 and 24 h. The normalized scattered light intensity was calculated by dividing by the peak maximum of the nontreated samples.

formation of heterogeneous structures was observed after incubation with 0.03 and 0.1 wt %  $H_2O_2$ , showing destabilization of the micellar structure by  $H_2O_2$  oxidation.

# **3.6. Cytotoxicity of the Doxorubicin-Loaded Micelles.** To test the feasibility of the micelles for cancer-selective drug release, we loaded the anticancer drug doxorubicin (Dox) into micelles and evaluated the toxicity in cancer and normal cells. For this experiment, we used micelle 3d, which can keep the micellar structure at room temperature (about 25 °C) due to its low LCST of 17.3 °C. Since micelles 3b and 3c dissociate into unimers at room temperature, those micelles are unlikely to be useful for practical applications.

The Dox-loaded micelles (Dox/3d) were prepared by mixing the polymer solution at different Dox concentrations followed by subsequent filtration through a 0.22  $\mu$ m syringe

filter. The optimum concentration of Dox was determined by monitoring the size change, as determined by DLS. As shown in Figure 6a, the micelle size increased upon the addition of

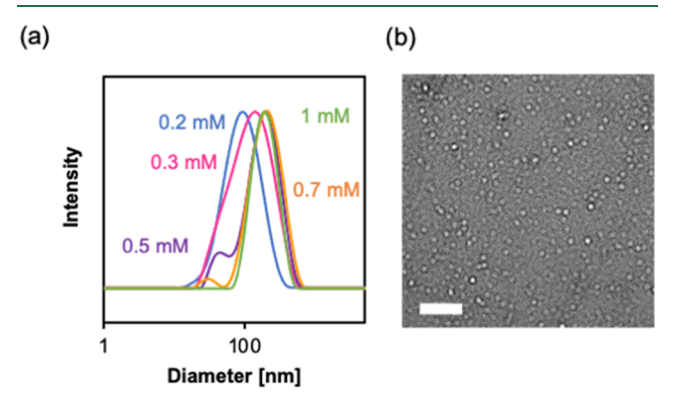


**Figure 6.** Encapsulation of Dox in the micelles. (a) Micelle size distribution of Dox/3d as measured by DLS. Polymer 3d (6 mg/mL) in distilled water was mixed with Dox (0.2–1 mM) at 37 °C and filtered through a 0.22  $\mu$ m syringe filter before measurement. (b) Negative staining TEM image of the Dox/3d micelle (0.2 mM Dox). Scale bar: 200 nm.

Dox. The diameter of the micelles reached 175.3 nm when 6 mg/mL polymer was mixed with 1 mM Dox. We did not observe obvious precipitations in the solution up to 1 mM, indicating that this increase in the micelle size is due to the encapsulation of Dox within the micellar core. The spherical morphology of the Dox/3d micelles was observed by negative staining TEM (Figure 6b). Although the high drug loading is beneficial, polymeric micelles larger than 200 nm may not be

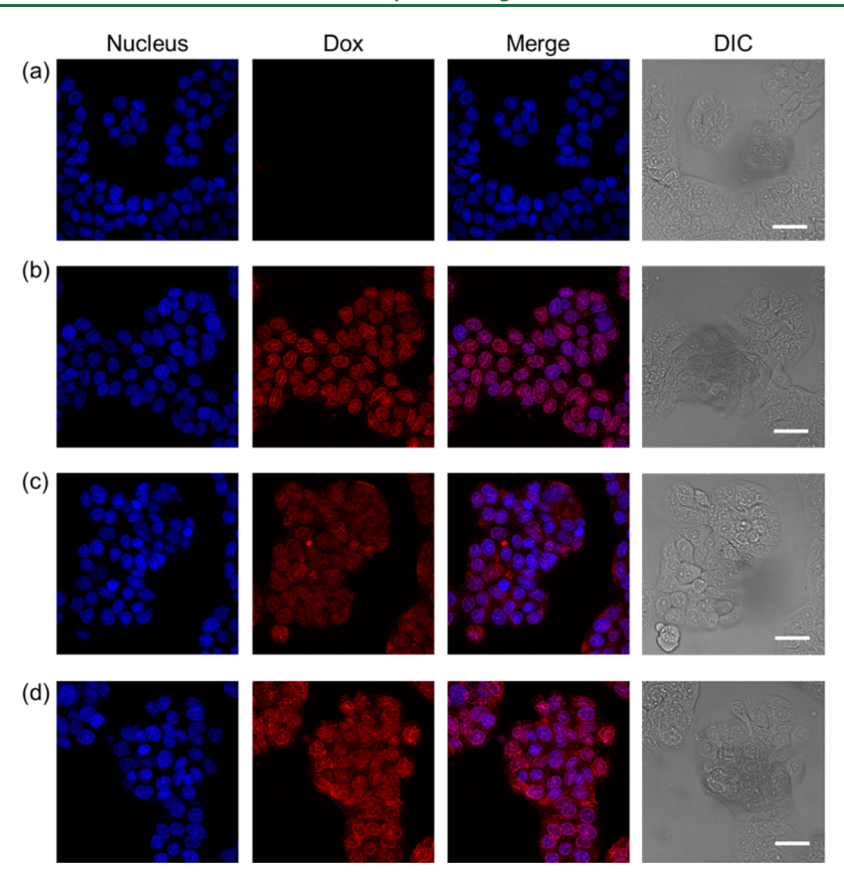
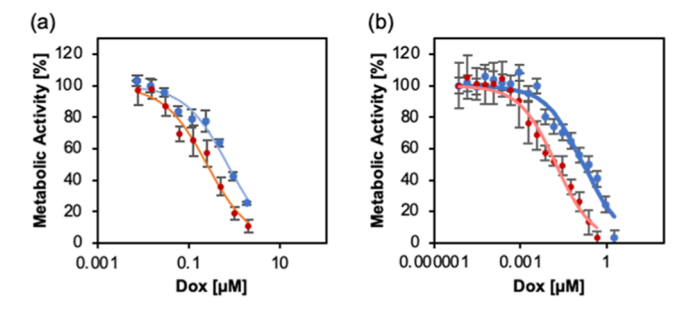


Figure 7. CLSFM images of Dox in HT29 cells. Cells were cultured in the presence of Dox or Dox/3d for 1.5 and 3 h. (a) Nontreated, (b) Dox for 1.5 h, and Dox/3d for (c) 1.5 and (d) 3 h. The nucleus was stained with Hoechst 33342. Dox:  $10 \mu M$ . Scale bar:  $30 \mu m$ .

suited for drug delivery as it is known that large nanoparticles are readily captured by phagocytes. Therefore, we decided to use the Dox/3d micelles prepared at 0.2 mM Dox ( $D_{\rm h}$  = 80.95 nm, PDI = 0.24) for the following *in vitro* experiments.

Intracellular localization of Dox encapsulated in the 3d micelles was observed by confocal laser scanning fluorescence microscopy (CLSFM). As shown in Figure 7a, cells treated with free Dox showed strong red fluorescence of Dox in the nucleus after 1.5 h of culture. For the Dox-loaded micelles, we observed red fluorescence of Dox spread within the cytosol along with the weaker fluorescence in the nucleus after 1.5 h. Since the micelles are known to be taken up by cells via endocytosis and localize within endo/lysosomes, 35 it is likely that the fluorescence observed in the nucleus is due to free Dox released from the micelles, while the fluorescence in the cytosol where endo/lysosomes exist is due to Dox encapsulated in the micelles. Therefore, the result indicates that the majority of Dox was maintained within the micelles after 1.5 h. On the other hand, after 3 h of culture, the fluorescence in the nucleus became intense compared to that in the cytosol, implying that a significant amount of Dox was released from the micelles.

The cytotoxicity of the Dox/3d micelles was evaluated in HT29 cells, as well as in HUVECs. Cells were cultured in the presence of the Dox/3d micelles and Dox for 3 days. The metabolic activity of cells was measured by MTT assay, and the IC<sub>50</sub> values were determined (Figure 8 and Table 5). Then, the IC<sub>50</sub> ratios (IC<sub>50</sub>(HUVEC)/IC<sub>50</sub>(HT29)), where a higher IC<sub>50</sub> ratio means enhanced toxicity in HT29 cells and/or reduced toxicity in HUVECs, were determined to evaluate the relative cytotoxicity in HT29 cells over HUVECs. As shown in



**Figure 8.** Cytotoxicity of Dox-loaded micelles in (a) HT29 cells and (b) HUVECs. Cells were cultured in the presence of Dox-HCl (red) and Dox/3d (blue) for 3 days. Cell viability was measured by MTT assay, n = 3.

Table 5. IC<sub>50</sub> of Dox-Loaded Micelles

	$IC_{50} [\mu M]$		
entry	HT29	HUVEC	relative toxicity $IC_{50(HUVEC)}/IC_{50~(HT29)}$
Dox	0.26	0.018	0.069
Dox/3d	0.70	0.16	0.23

Table 5, the Dox/3d micelles showed a much higher IC $_{50}$  ratio compared to Dox, indicating that the micelles released Dox selectively in HT29 cells over HUVECs. Furthermore, 3d micelles without Dox did not show obvious toxicity in both HT29 cells and HUVECs at the concentration range used for the cytotoxicity assay (Figure S31). We also tested the cytotoxicity of the Dox/3a micelles, which do not contain the oxidation-sensitive TMAM units, in HT29 cells (Figure S32)

and Table S4). The IC $_{50}$  value was 0.73  $\mu$ M, which is similar to that of Dox/3d (0.70  $\mu$ M). As discussed above, the micelles dissociate and release Dox at room temperature since the LCST of 3a is 32 °C. Therefore, this result is likely to be due to partial dissociation of the 3a micelle during the formulation handling, which was done at room temperature (outside the CO $_2$  incubator).

#### 4. CONCLUSIONS

We herein report the oxidation-sensitive micelles with a controlled dissociation rate. The copolymers of NIPAM and TMAM showed significant changes in their LCSTs upon oxidation. The LCST of the P(NIPAM/TMAM) copolymers decreased with an increase in the TMAM content. Upon oxidation, the LCST increased above 35 °C. Due to this LCST change, P(NIPAM/TMAM) undergoes a globule-to-coil transition upon oxidation at 37 °C. The micelles with a core comprising a P(NIPAM/TMAM) block showed fast dissociation compared to the micelles with a PTMAM core. The fastest dissociation rate was observed for the micelles with the NIPAM:TMAM ratio of 97:3 followed in order of 90:10 and 82:18. The doxorubicin (Dox)-loaded micelles showed high relative toxicity in HT29 cells over HUVECs, indicating the selective release of Dox in cells under oxidative stress conditions. The results clearly show the potential of the P(NIPAM/TMAM) copolymers as oxidation-sensitive building blocks for designing cancer-targeted drug delivery systems.

# ASSOCIATED CONTENT

### Supporting Information

The Supporting Information is available free of charge at https://pubs.acs.org/doi/10.1021/acs.biomac.3c01156.

Experimental details (materials, instrumentation, and synthetic procedure), <sup>1</sup>H NMR spectra, GPC elution profiles, DLS results, TEM images, and cytotoxicity assay results (PDF)

#### AUTHOR INFORMATION

#### **Corresponding Author**

Urara Hasegawa — Department of Materials Science and Engineering, The Pennsylvania State University, University Park, Pennsylvania 16802, United States; ⊙ orcid.org/0000-0002-4189-7630; Email: uph5002@psu.edu

#### **Authors**

Roujia Chang – Department of Materials Science and Engineering, The Pennsylvania State University, University Park, Pennsylvania 16802, United States

Binru Han – Department of Materials Science and Engineering, The Pennsylvania State University, University Park, Pennsylvania 16802, United States

Amira Ben Mabrouk – Department of Materials Science and Engineering, The Pennsylvania State University, University Park, Pennsylvania 16802, United States

Complete contact information is available at: https://pubs.acs.org/10.1021/acs.biomac.3c01156

# **Author Contributions**

The manuscript was written through contributions of all authors. All authors have given approval to the final version of the manuscript.

#### **Notes**

The authors declare no competing financial interest.

# ACKNOWLEDGMENTS

We appreciate Dr. André J. van der Vlies (Penn State) for synthesizing the TMAM monomer. This work was supported by the National Science Foundation (NSF), CBET, 2102848.

#### ABBREVIATIONS

PAM, poly(*N*-acryloyl morpholine); TMAM, thiomorpholine acrylamide; NIPAM, *N*-isopropylacrylamide; ROS, reactive oxygen species; LCST, low critical solution temperature

#### REFERENCES

- (1) Liou, G. Y.; Storz, P. Reactive oxygen species in cancer. Free Radical Res. 2010, 44 (5), 479-496.
- (2) Nakamura, H.; Takada, K. Reactive oxygen species in cancer: Current findings and future directions. *Cancer Sci.* **2021**, *112* (10), 3945–3952.
- (3) Cheung, E. C.; Vousden, K. H. The role of ROS in tumour development and progression. *Nat. Rev. Cancer* **2022**, 22 (5), 280–297
- (4) Pelicano, H.; Carney, D.; Huang, P. ROS stress in cancer cells and therapeutic implications. *Drug Resistance Updates* **2004**, *7* (2), 97–110.
- (5) Jia, P.; Dai, C.; Cao, P.; Sun, D.; Ouyang, R.; Miao, Y. The role of reactive oxygen species in tumor treatment. *RSC Adv.* **2020**, *10* (13), 7740–7750 10.1039/C9RA10539E.
- (6) Sullivan, L. B.; Chandel, N. S. Mitochondrial reactive oxygen species and cancer. *Cancer Metab.* **2014**, *2*, 17.
- (7) Sies, H. Hydrogen peroxide as a central redox signaling molecule in physiological oxidative stress: Oxidative eustress. *Redox Biol.* **2017**, *11*, 613–619.
- (8) Marinho, H. S.; Real, C.; Cyrne, L.; Soares, H.; Antunes, F. Hydrogen peroxide sensing, signaling and regulation of transcription factors. *Redox Biol.* **2014**, *2*, 535–562.
- (9) Denu, J. M.; Tanner, K. G. Specific and reversible inactivation of protein tyrosine phosphatases by hydrogen peroxide: evidence for a sulfenic acid intermediate and implications for redox regulation. *Biochemistry* **1998**, *37* (16), 5633–5642.
- (10) Mehdi, M. Z.; Azar, Z. M.; Srivastava, A. K. Role of receptor and nonreceptor protein tyrosine kinases in H2O2-induced PKB and ERK1/2 signaling. *Cell Biochem. Biophys.* **2007**, 47 (1), 1–10.
- (11) Cerritelli, S.; O'Neil, C. P.; Velluto, D.; Fontana, A.; Adrian, M.; Dubochet, J.; Hubbell, J. A. Aggregation behavior of poly-(ethylene glycol-bl-propylene sulfide) di- and triblock copolymers in aqueous solution. *Langmuir* **2009**, 25 (19), 11328–11335.
- (12) Dane, K. Y.; Nembrini, C.; Tomei, A. A.; Eby, J. K.; O'Neil, C. P.; Velluto, D.; Swartz, M. A.; Inverardi, L.; Hubbell, J. A. Nano-sized drug-loaded micelles deliver payload to lymph node immune cells and prolong allograft survival. *J. Controlled Release* **2011**, *156* (2), 154–160.
- (13) Wei, C.; Liang, B.; Li, Y.; Yan, B.; Zhou, Y.; Liu, Y.; Lang, M. A Drug-Free Therapeutic System for Cancer Therapy by Diselenide-Based Polymers Themselves. *Adv. Healthcare Mater.* **2021**, *10* (2), No. 2001471.
- (14) Deepagan, V. G.; Kwon, S.; You, D. G.; Nguyen, V. Q.; Um, W.; Ko, H.; Lee, H.; Jo, D. G.; Kang, Y. M.; Park, J. H. In situ diselenide-crosslinked polymeric micelles for ROS-mediated anticancer drug delivery. *Biomaterials* **2016**, *103*, 56–66.
- (15) Wang, L.; Wang, W.; Cao, W.; Xu, H. Multi-hierarchical responsive polymers: stepwise oxidation of a selenium- and tellurium-containing block copolymer with sensitivity to both chemical and electrochemical stimuli. *Polym. Chem.* **2017**, 8 (31), 4520–4527 10.1039/C7PY00971B.
- (16) Ge, C.; Zhu, J.; Wu, G.; Ye, H.; Lu, H.; Yin, L. ROS-Responsive Selenopolypeptide Micelles: Preparation, Characterization, and

Controlled Drug Release. Biomacromolecules 2022, 23 (6), 2647–2654.

- (17) Han, P.; Ma, N.; Ren, H.; Xu, H.; Li, Z.; Wang, Z.; Zhang, X. Oxidation-responsive micelles based on a selenium-containing polymeric superamphiphile. *Langmuir* **2010**, 26 (18), 14414–14418. (18) Yadav, S.; Kumar, P.; Jo, S.-H.; Park, S.-H.; Lee, W.-K.; Yoo, S., II; Lim, K. T. Redox-responsive properties of core-cross-linked micelles of poly(ethylene oxide)-b-poly(furfuryl methacrylate) for anticancer drug delivery application. *React. Funct. Polym.* **2022**, 175, No. 105271.
- (19) Ma, N.; Li, Y.; Ren, H.; Xu, H.; Li, Z.; Zhang, X. Selenium-containing block copolymers and their oxidation-responsive aggregates. *Polym. Chem.* **2010**, *1* (10), 1609–1614 10.1039/C0PY00144A. (20) Cao, W.; Gu, Y.; Li, T.; Xu, H. Ultra-sensitive ROS-responsive tellurium-containing polymers. *Chem. Commun.* **2015**, *51* (32), 7069–7071.
- (21) Wang, L.; Fan, F.; Cao, W.; Xu, H. Ultrasensitive ROS-Responsive Coassemblies of Tellurium-Containing Molecules and Phospholipids. ACS Appl. Mater. Interfaces 2015, 7 (29), 16054–16060.
- (22) Lennicke, C.; Rahn, J.; Lichtenfels, R.; Wessjohann, L. A.; Seliger, B. Hydrogen peroxide—production, fate and role in redox signaling of tumor cells. *Cell Commun. Signaling* **2015**, *13* (1), 39.
- (23) Stein, K. T.; Moon, S. J.; Nguyen, A. N.; Sikes, H. D. Kinetic modeling of H2O2 dynamics in the mitochondria of HeLa cells. *PLoS Comput. Biol.* **2020**, *16* (9), e1008202.
- (24) Lyublinskaya, O.; Antunes, F. Measuring intracellular concentration of hydrogen peroxide with the use of genetically encoded H2O2 biosensor HyPer. *Redox Biol.* **2019**, 24, No. 101200.
- (25) van der Vlies, A. J.; Xu, J.; Ghasemi, M.; Bator, C.; Bell, A.; Rosoff-Verbit, B.; Liu, B.; Gomez, E. D.; Hasegawa, U. Thioether-Based Polymeric Micelles with Fine-Tuned Oxidation Sensitivities for Chemotherapeutic Drug Delivery. *Biomacromolecules* **2022**, 23 (1), 77–88.
- (26) Takei, Y. G.; Aoki, T.; Sanui, K.; Ogata, N.; Okano, T.; Sakurai, Y. Temperature-responsive bioconjugates. 2. Molecular design for temperature-modulated bioseparations. *Bioconjugate Chem.* 1993, 4 (5), 341–346.
- (27) Jain, K.; Vedarajan, R.; Watanabe, M.; Ishikiriyama, M.; Matsumi, N. Tunable LCST behavior of poly(N-isopropylacrylamide/ionic liquid) copolymers. *Polym. Chem.* **2015**, *6* (38), *6*819–6825.
- (28) Li, S.; Chung, H. S.; Simakova, A.; Wang, Z.; Park, S.; Fu, L.; Cohen-Karni, D.; Averick, S.; Matyjaszewski, K. Biocompatible Polymeric Analogues of DMSO Prepared by Atom Transfer Radical Polymerization. *Biomacromolecules* **2017**, *18* (2), 475–482.
- (29) Kaneko, Y.; Nakamura, S.; Sakai, K.; Aoyagi, T.; Kikuchi, A.; Sakurai, Y.; Okano, T. Rapid Deswelling Response of Poly(Nisopropylacrylamide) Hydrogels by the Formation of Water Release Channels Using Poly(ethylene oxide) Graft Chains. *Macromolecules* 1998, 31 (18), 6099–6105.
- (30) Okuyama, Y.; Yoshida, R.; Sakai, K.; Okano, T.; Sakurai, Y. Swelling controlled zero order and sigmoidal drug release from thermo-responsive poly(N-isopropylacrylamide-co-butyl methacrylate) hydrogel. *J. Biomater. Sci., Polym. Ed.* **1993**, 4 (5), 545–556.
- (31) Okano, T.; Bae, Y. H.; Jacobs, H.; Kim, S. W. Thermally on-off switching polymers for drug permeation and release. *J. Controlled Release* **1990**, *11* (1), 255–265.
- (32) Valencia, L.; Enríquez, F. J.; Valencia, M.; Díaz, R. Tuning the LCST of PNIPAM via Random Oxidation-Sensitive Thioether Functionalities. *Macromol. Chem. Phys.* **2017**, *218* (9), 1600556.
- (33) Gustafson, H. H.; Holt-Casper, D.; Grainger, D. W.; Ghandehari, H. Nanoparticle Uptake: The Phagocyte Problem. *Nano Today* **2015**, *10* (4), 487–510.
- (34) Alqahtani, M. S.; Syed, R.; Alshehri, M. Size-Dependent Phagocytic Uptake and Immunogenicity of Gliadin Nanoparticles. *Polymers* **2020**, *12* (11), 2576.
- (35) Qiu, C.; Xia, F.; Zhang, J.; Shi, Q.; Meng, Y.; Wang, C.; Pang, H.; Gu, L.; Xu, C.; Guo, Q.; Wang, J. Advanced Strategies for Over

coming Endosomal/Lysosomal Barrier in Nanodrug Delivery. Research 2023, 6, No. 0148.

ī